THE CRYSTAL STRUCTURE OF BERTOSSAITE, CaLi$_2$[Al$_4$(PO$_4$)$_4$(OH,F)$_4$]

Frédéric HATERT[§], Pierre LEFÈVRE and André-Mathieu FRANSOLET

Laboratoire de Minéralogie, B18, Université de Liège, B–4000 Liège, Belgium

ABSTRACT

A sample of bertossaite {CaLi$_2$[Al$_4$(PO$_4$)$_4$(OH,F)$_4$]} from the Buranga pegmatite, Rwanda, was investigated by single-crystal X-ray diffraction, electron microprobe, and infrared spectroscopic techniques. Under the polarizing microscope, bertossaite forms large xenomorphic grains reaching 500 μm in length, included in montebrasite and associated with quartz and a phosphate of the lazulite–scorzalite series. Electron-microprobe analyses indicate the empirical formula (Ca$_{0.83}$Na$_{0.15}$Sr$_{0.02}$)$_{\Sigma1.00}$(Li$_{1.86}$Mn$_{0.10}$ Na$_{0.04}$)$_{\Sigma2.00}$[(Al$_{3.90}$Fe$_{0.09}$Mg$_{0.01}$)$_{\Sigma4.00}$(PO$_4$)$_4$(OH$_{3.35}$F$_{0.65}$)$_{\Sigma4.00}$]; the mechanism of coupled substitution Li$^+$ + Ca^{2+} = Mn^{2+} + Na$^+$ explains the presence of Na at the *Ca* site and of Mn at the *Li* site. The crystal structure of bertossaite [*Imcb*, *a* 11.476(1), *b* 15.744(1), *c* 7.228(1) Å] is isotypic with that of palermoite {SrLi$_2$[Al$_4$(PO$_4$)$_4$(OH)$_4$]}, and is based on dimers of edge-sharing AlO$_6$ octahedra, which are connected together *via* corner-sharing to form chains of octahedra running along the **a** axis. These chains are connected to adjacent chains by corner-sharing PO$_4$ tetrahedra, constituting a heteropolyhedral framework that contains large channels in which the Ca and Li atoms occur. A comparison between the OH…O distances calculated from the infrared spectrum, and those obtained from the structural data, allows one to assign the bands corresponding to the stretching vibrations of the (OH) groups.

Keywords: bertossaite, Li–Al–Ca-bearing phosphate, crystal structure, infrared spectroscopy, Buranga pegmatite, Rwanda.

SOMMAIRE

Un échantillon de bertossaïte {CaLi$_2$[Al$_4$(PO$_4$)$_4$(OH,F)$_4$]} provenant de la pegmatite de Buranga, Rwanda, a été étudié par diffraction des rayons X sur monocristal, en spectroscopie infrarouge, et a fait l'objet d'analyses chimiques à la microsonde électronique. Sous le microscope polarisant, la bertossaïte se présente en grains atteignant 500 μm de longueur, inclus dans la montebrasite et associés au quartz et à un phosphate de la série lazulite–scorzalite. Les analyses chimiques à la microsonde électronique conduisent à la formule (Ca$_{0.83}$Na$_{0.15}$Sr$_{0.02}$)$_{\Sigma1.00}$(Li$_{1.86}$Mn$_{0.10}$Na$_{0.04}$)$_{\Sigma2.00}$[(Al$_{3.90}$Fe$_{0.09}$Mg$_{0.01}$)$_{\Sigma4.00}$(PO$_4$)$_4$(OH$_{3.35}$ F$_{0.65}$)$_{\Sigma4.00}$], et le mécanisme de substitution Li$^+$ + Ca^{2+} = Mn^{2+} + Na$^+$ permet d'expliquer la présence de Na sur le site Ca, et de Mn sur le site Li. La structure cristalline de la bertossaïte [*Imcb*, *a* 11.476(1), *b* 15.744(1), *c* 7.228(1) Å] est identique à celle de la palermoïte {SrLi$_2$[Al$_4$(PO$_4$)$_4$(OH)$_4$]}, et est caractérisée par la présence de dimères formés par deux octaèdres AlO$_6$ partageant une arête. Ces dimères sont connectés entre eux par les sommets, et forment ainsi des chaînes d'octaèdres parallèles à l'axe cristallographique **a**. Ces chaînes sont connectées aux chaînes adjacentes par des tétraèdres PO$_4$, formant ainsi une charpente contenant de larges canaux dans lesquels se logent Ca et Li. Une comparaison entre les distances OH…O calculées à partir du spectre infrarouge, et celles obtenues lors de l'affinement structural, a permis d'attribuer les bandes d'absorption correspondant aux vibrations des différents groupements (OH).

Mots-clés: bertossaïte, phosphate de Li–Ca–Al, structure cristalline, spectroscopie infrarouge, pegmatite de Buranga, Rwanda.

INTRODUCTION

Bertossaite, CaLi$_2$[Al$_4$(PO$_4$)$_4$(OH,F)$_4$], was originally described by von Knorring (1965) and von Knorring & Mrose (1966) in the Buranga pegmatite, Rwanda, in association with augelite [Al$_2$(PO$_4$) (OH)$_3$], brazilianite [NaAl$_3$(PO$_4$)$_2$(OH)$_4$], lazulite [MgAl$_2$(PO$_4$)$_2$(OH)$_2$], and muscovite. On the basis of a preliminary X-ray diffraction and chemical investi-gation, von Knorring (1965) concluded that the new phosphate corresponds to the Ca analogue of paler-moite, SrLi$_2$[Al$_4$(PO$_4$)$_4$(OH)$_4$]. The physical properties of bertossaite were then determined by von Knorring & Mrose (1966), who measured the unit-cell parameters, *a* 11.48(1), *b* 15.73(2), and *c* 7.23(1) Å, extinction symbol *I*aa*.

The crystal structure of palermoite was determined by Moore & Araki (1975), who showed that it is closely

related to that of carminite, $Pb_2[Fe_4(AsO_4)_4(OH)_4]$, earlier determined by Finney (1963). The unit-cell parameters obtained by Moore & Araki (1975) are *a* 11.556(5), *b* 15.847(7), and *c* 7.315(4) Å, space group *Imcb*. The only difference between the palermoite and carminite structures resides in the position of the Li atom in palermoite, which is significantly displaced from the Pb(2) special position of carminite, thus inducing a doubling of the Li-site multiplicity. As also mentioned by von Knorring & Mrose (1966), bertossaite and palermoite are also homeotypic with attakolite, $CaMn^{2+}[Al_4(HSiO_4)(PO_4)_3(OH)_4]$; the structural investigation of attakolite confirmed this hypothesis (Grice & Dunn 1992).

Recently, Lefèvre (2003) investigated new samples of phosphates from the Rubindi and Kabilizi pegmatites, Rwanda, and discovered a new occurrence of bertossaite in veins cross-cutting montebrasite $[LiAl(PO_4) OH]$, scorzalite $[(Fe,Mg)Al_2(PO_4)_2(OH)_2]$, and brazilianite. These veins appeared during the hydrothermal transformation phase affecting these pegmatites, before the replacement of montebrasite by trolleite $[Al_4(PO_4)_3(OH)_3]$. That study motivated a detailed mineralogical investigation of bertossaite, including sample BU–AL–2 from the Buranga pegmatite, which was given by O. von Knorring to A.-M. Fransolet. It can consequently be considered as a cotype. A good-quality single crystal of bertossaite was extracted from this sample, giving us the opportunity to investigate the still unknown structure of this rare phosphate mineral. The results of this structure refinement, as well as new electron-microprobe analyses and infrared spectral measurements, are given and discussed in the present paper.

EXPERIMENTAL

Electron-microprobe analyses (Table 1) were carried out with a Cameca SX–50 instrument (Université de Louvain-la-Neuve, Belgium) operating in the wavelength-dispersion mode, with an accelerating voltage of 15 kV and a beam current of 20 nA. The following standards were used: graftonite (P, Mn, Fe), corundum (Al), olivine (Mg), wollastonite (Ca), oligoclase (Na), leucite (K), strontianite (Sr), barite (Ba), and synthetic LiF (F). The counting time was 15 s for Sr and Al, and 10 s for the other elements. The X-ray structural study was carried out on a Bruker P4 four-circle diffractometer (Mo$K\alpha$ radiation, $\lambda = 0.71073$ Å), on a crystal fragment measuring $0.30 \times 0.13 \times 0.08$ mm. The unit-cell parameters and standard deviations were calculated for the setting angles of 37 reflections with $12.3° < 2\theta < 25.0°$: *a* 11.476(1), *b* 15.744(1), and *c* 7.228(1) Å. The intensities of 1060 reflections, corresponding to 794 unique reflections ($R_{int} = 0.021$), were measured by the ω scan technique in the range $5.18° < 2\theta < 54.98°$ ($h = \bar{1} \rightarrow 14$, $k = \overline{20} \rightarrow 1$, $l = \bar{9} \rightarrow 1$). Data were corrected for Lorentz, polarization and absorption effects, the latter with a semi-empirical method using a reliable set of Ψ-scan data.

The crystal structure was refined in the space group *Imcb*, which is in accordance with the systematic absences, starting from the atomic coordinates of palermoite (Moore & Araki 1975). Cation occupancies were refined to obtain better agreement with the chemical composition measured with an electron microprobe on a thin section from the same sample (Table 1). For the sake of simplicity, Fe^{2+}, Mg, K, Sr, and Ba, which are present in very low amounts, were not taken into account in the structure refinement. Also, in spite of some F-for-OH substitution, the presence of F was not taken into account in the least-squares model. Finally, the relative occupancies of Ca and Na at the Ca site, and of Al and vacancies at the Al site, were refined. The occurrence of a significant electron-density close to the Li position forced us to use a split-atom model, in which 0.51 Li, 0.07 Na, and 0.05 Mn were constrained on the Li(1) site, whereas 0.42 Li were constrained on the Li(2) position. Hydrogen atoms were located in a final difference-Fourier map, and the refinement procedure was completed using anisotropic displacement parameters for all non-H atoms, except for the atoms occurring at the Li(1) and Li(2) sites, which showed strongly anisotropic displacement parameters. The final conventional R_1 factor was 0.0285. Further details concerning the collection of intensity data and the refinement procedure are given in Table 2. A table of structure factors and a cif file are available from the Depository of Unpublished Data on the Mineralogical Association of Canada website [document Bertossaite CM49_1079].

The infrared spectrum of bertossaite was recorded with a Nicolet NEXUS spectrometer, from 32 scans

TABLE 1. CHEMICAL COMPOSITION OF BERTOSSAITE FROM BURANGA, RWANDA

	1	2		1	2
P_2O_5 wt.%	45.34	46.34	P *apfu*	4.000	4.000
Al_2O_3	33.42	32.44	Al	4.105	3.898
MgO	-	0.08	Mg	-	0.011
FeO	0.98	1.06	Fe	0.085	0.091
MnO	0.76	1.17	Mn	0.067	0.101
CaO	8.36	7.56	Ca	0.933	0.826
SrO	-	0.38	Sr	-	0.022
BaO	-	0.06	Ba	-	0.002
Na_2O	0.34	0.96	Na	0.069	0.190
K_2O	-	0.01	K	-	0.001
Li_2O	4.21	4.53*	Li	1.765	1.859
H_2O	5.36	4.93*	OH	3.726	3.353
F	1.68	2.01	F	0.554	0.647
O=F	0.71	0.85			
Total	99.74	100.68			

1. Results of a wet-chemical analysis from von Knorring (1965). Cation numbers are calculated on the basis of 4 P atoms per formula unit. 2. Average result of 17 point analyses acquired with an electron microprobe (J. Wautier, analyst). The Li_2O and H_2O values (*) were calculated from the ideal formula of bertossaite, taking into account the OH = F and Li = (Na,Mn) mechanisms of substitution.

with a 1 cm^{-1} resolution, between 400 and 4000 cm^{-1}. The sample was prepared by thoroughly mixing 2 mg of sample with KBr in order to obtain a 150 mg homogeneous pellet, which was subsequently dried for several hours at 120°C. To prevent water contamination, the measurements were performed under a dry air purge.

THE CHEMICAL COMPOSITION OF BERTOSSAITE

Sample BU–AL–2, collected from the Buranga pegmatite, was examined under the polarizing microscope; it shows the presence of large xenomorphic grains of bertossaite reaching 500 μm in length (Fig. 1). Bertossaite is included in montebrasite, and both minerals are associated with quartz and a phosphate of the lazulite–scorzalite series. Electron-microprobe analyses of bertossaite (Table 1) were interpreted on the basis of four P atoms per formula unit, and indicate the empirical formula $(Ca_{0.83}Na_{0.15}Sr_{0.02})_{\Sigma 1.00}$ $(Li_{1.86}Mn_{0.10}Na_{0.04})_{\Sigma 2.00}[(Al_{3.90}Fe_{0.09}Mg_{0.01})_{\Sigma 4.00}(PO_4)_4$ $(OH_{3.35}F_{0.65})_{\Sigma 4.00}]$. This formula is in good agreement with the ideal formula of bertossaite, and with the composition measured by von Knorring (1965) on the type specimen (Table 1).

As shown in Figure 2, a very good correlation exists between the Na and Ca contents of bertossaite, with a slope close to –1. This correlation indicates that Ca^{2+} is replaced by Na^+ in the structure; however, owing to the different valence states of these cations, this substitution is associated with a replacement of Li^+ by Mn^{2+},

leading to the coupled substitution mechanism $Li^+ + Ca^{2+} = Mn^{2+} + Na^+$. This mechanism of substitution explains the presence of Na at the Ca site, and of Mn at the Li site, detected by the single-crystal structure refinement (see below).

REFINEMENT OF THE STRUCTURE

Final positional and equivalent isotropic displacement parameters for bertossaite are given in Table 3, and selected bond-distances and angles are given in Table 4. The main features of the bertossaite structure are identical to those of palermoite (Moore & Araki 1975). The basic unit of the structure consists of dimers of edge-sharing AlO_6 octahedra, which are connected *via* corner-sharing to form chains of octahedra running along the **a** axis (Fig. 3). These chains are connected to adjacent chains by corner-sharing PO_4 tetrahedra,

TABLE 3. FINAL FRACTIONAL COORDINATES AND EQUIVALENT ISOTROPIC DISPLACEMENT PARAMETERS (Å^2) OF ATOMS IN BERTOSSAITE FROM BURANGA

Site	x	y	z	U_{eq}
Li(1)	0.5	0.2851(3)	0.2334(9)	0.020(1)
Li(2)	0.5	0.2814(9)	0.320(2)	0.008(3)
Ca	0.25	0.5	0.5	0.0106(4)
Al	0.13082(6)	0.37439(4)	0.1405(1)	0.0052(2)
P(1)	0.25	0.29109(5)	0.5	0.0054(2)
P(2)	0	0.45694(5)	0.7681(1)	0.0056(2)
O(1)	0.1427(1)	0.2657(1)	0.0331(2)	0.0101(4)
O(2)	0.2294(1)	0.3512(1)	0.3364(2)	0.0106(4)
O(3)	0	0.3938(2)	0.6123(4)	0.0117(5)
O(4)	0	0.4049(1)	0.9558(3)	0.0078(5)
O(5)	0.1096(1)	0.4861(1)	0.2399(2)	0.0082(4)
OH(1)	0	0.3368(2)	0.2648(3)	0.0076(5)
OH(2)	0.25	0.4129(2)	0	0.0052(4)
H(1)	0	0.3572	0.3789	0.03(1)
H(2)	0.25	0.4498	0	0.04(2)

TABLE 2. EXPERIMENTAL DETAILS FOR THE SINGLE-CRYSTAL X-RAY-DIFFRACTION STUDY OF BERTOSSAITE FROM BURANGA

Dimensions of the crystal (mm)	*ca.* 0.30 × 0.13 × 0.08
Unit-cell parameters	
a (Å)	11.476(1)
b (Å)	15.744(1)
c (Å)	7.228(1)
Space group	*Imcb*
Z	4
Calculated density (g/cm^3)	3.183
Diffractometer	Bruker P4
Operating conditions	50 kV, 30 mA
Radiation	MoKα (λ = 0.71073 Å)
Scan mode	ω scan
$2\theta_{min}, 2\theta_{max}$	5.18°, 54.98°
Range of indices	$-1 \leq h \leq 14, -20 \leq k \leq 1, -9 \leq l \leq 1$
Measured intensities	1060
Unique reflections	794
Independent non-zero [$I > 2\sigma(I)$] reflections	720
Absorption correction	Semi-empirical
μ (mm^{-1})	1.619
T_{min}, T_{max}	0.877, 0.994
l.s. refinement program	SHELXL-93 (Sheldrick 2008)
Refined parameters	85
R_1 [$I > 2\sigma(I)$]	0.0285
R_1 (all)	0.0321
wR_2 (all)	0.0757
S (goodness of fit)	1.263
Max Δ/σ in the last l.s. cycle	0.000
Max peak and hole in the final ΔF map (e/Å^3)	+0.579 and −0.932

TABLE 4. SELECTED BOND-DISTANCES (Å) AND ANGLES (°) IN BERTOSSAITE FROM BURANGA

|					
P(1)-O(2)	× 2	1.533(2)	Li(1)-OH(1)		1.919(6)
P(1)-O(1)	× 2	1.541(2)	Li(1)-O(3)		2.043(6)
Mean		1.537	Li(1)-O(4)		2.329(6)
			Li(1)-O(1)	× 2	2.484(5)
O(2)-P(1)-O(2)		103.8(2)	Li(1)-O(1)'	× 2	2.546(5)
O(2)-P(1)-O(1)	× 2	111.2(1)	Mean		2.336
O(2)-P(1)-O(1)'	× 2	110.8(1)			
O(1)-P(1)-O(1)		109.0(1)	Ca-O(5)	× 4	2.486(2)
Mean		109.5	Ca-O(2)	× 4	2.635(2)
			Mean		2.561
P(2)-O(3)		1.502(2)			
P(2)-O(5)	× 2	1.546(2)	Al-OH(2)		1.808(1)
P(2)-O(4)		1.585(2)	Al-OH(1)		1.847(2)
Mean		1.545	Al-O(2)		1.849(2)
			Al-O(1)		1.884(2)
O(3)-P(2)-O(5)	× 2	110.8(1)	Al-O(5)		1.916(2)
O(5)-P(2)-O(5)		108.9(1)	Al-O(4)		2.065(2)
O(3)-P(2)-O(4)		107.4(1)	Mean		1.895
O(5)-P(2)-O(4)	× 2	109.4(1)			
Mean		109.5			
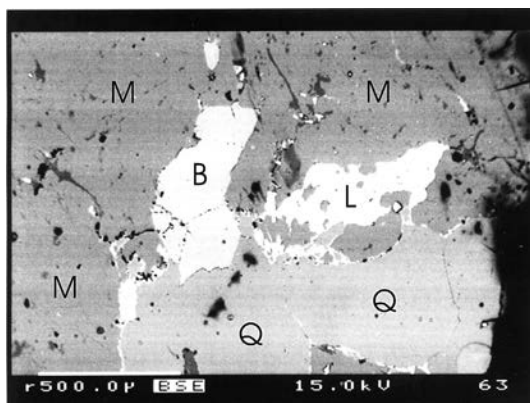
FIG. 1.   Mineral assemblage in sample BU–AL–2. Symbols: B: bertossaite, M: montebrasite, Q: quartz, L: lazulite–scorzalite. Scanning electron microscope image, back-scattered electron mode.

constituting a heteropolyhedral framework (Fig. 3). A view perpendicular to the **b** axis clearly shows the kinked profile of the chains (Fig. 4). The framework can be decomposed into slabs parallel to (010) (Fig. 3), between which occur the large cations distributed in Li- and Ca-rich layers alternating regularly along the **b** axis. A view perpendicular to the **a** axis (Fig. 5) shows that the framework also contains large channels, in which the Ca and Li atoms occur.

A detailed distribution of cations has also been established, by taking into account the results of the chemical analyses and of the single-crystal structure refinement. The results given in Table 5 indicate that the refined site-populations (RSP) obtained from the single-crystal structure refinement are in good agreement with the assigned site-populations (ASP) deduced from the electron-microprobe results. Moreover, the refined site-scattering values (RSS) and the mean bond-lengths (MBL) obtained from the structure refinement are very close to the calculated site-scattering values (CSS)
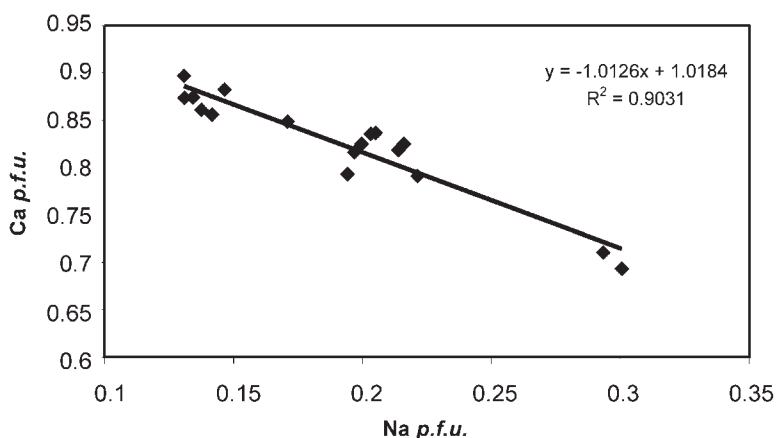

FIG. 2.   Correlation between the Ca and Na contents in bertossaite.

TABLE 5. REFINED SITE-POPULATIONS (RSP, *APFU*), REFINED SITE-SCATTERING
VALUES (RSS, *epfu*), MEAN BOND-LENGTHS (MBL, Å),
ASSIGNED SITE-POPULATIONS (ASP, *apfu*), CALCULATED SITE-SCATTERING
VALUES (CSS, *epfu*), AND CALCULATED BOND-LENGTHS (CBL, Å)
IN BERTOSSAITE FROM BURANGA

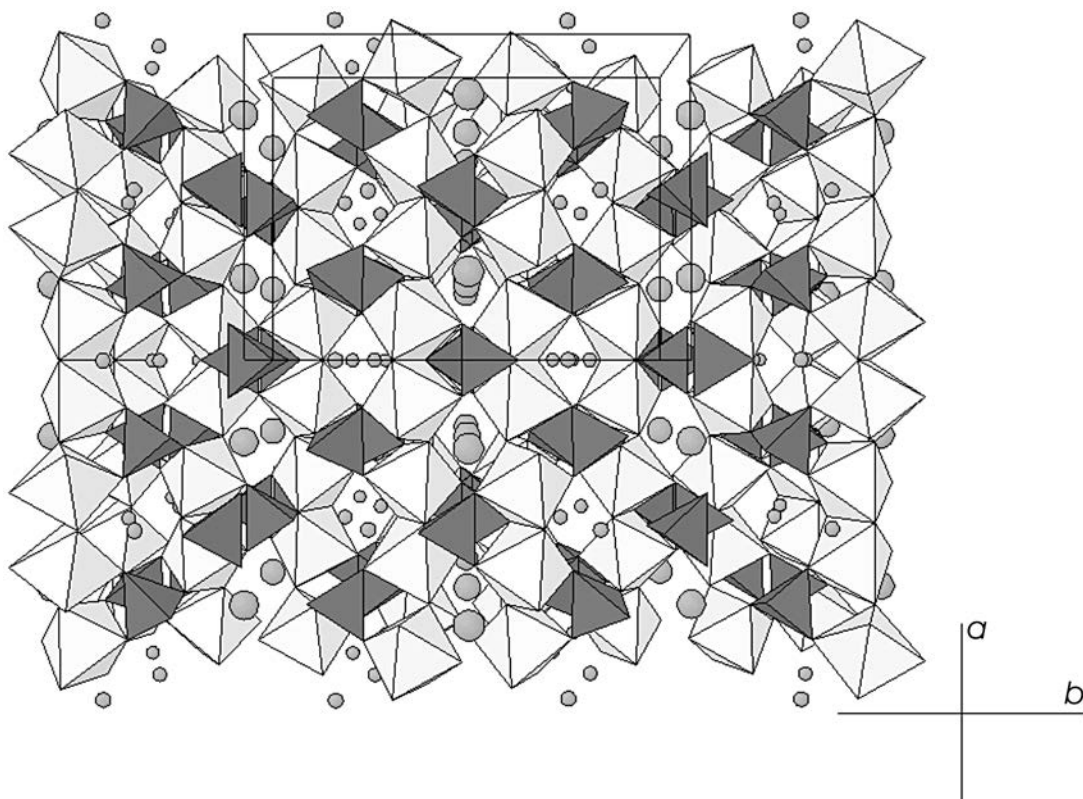| Site | Results of the structure determination | | | Results of the chemical analysis | | |
	RSP	RSS	MBL	ASP	CSS	CBL
Li(1), Li(2)	0.93 Li + 0.07 Na + 0.05 Mn	4.8	2.336	0.900 Li + 0.050 Mn^{2+} + 0.050 Na	4.5	2.280
Ca	0.87(1) Ca + 0.13(2) Na	18.8	2.561	0.870 Ca + 0.130 Na	18.8	2.548
Al	0.977(4) Al	12.7	1.895	0.975 Al + 0.025 Fe^{3+}	13.3	1.938

FIG. 3.   The crystal structure of bertossaite, projected along the **c** axis. The PO$_4$ tetrahedra are grey, and the AlO$_6$ octahedra are white. The large circles correspond to Ca atoms, and the small circles, to Li(1). For the sake of simplicity, Li(2) and hydrogen atoms are not shown.

TABLE 6. BOND-VALENCE TABLE (*vu*) FOR BERTOSSAITE
FROM BURANGA

	Li(1), Li(2)	Ca	Al	P(1)	P(2)	Σ
O(1)	0.26		0.54	1.23[*]		2.03
O(2)		0.16[**]	0.59	1.26[*]		2.01
O(3)	0.23				1.37	1.60
O(4)	0.11		0.33[***]	1.09		1.86
O(5)		0.23[**]	0.49		1.21[*]	1.93
OH(1)	0.32		0.59			0.91
OH(2)			0.66			0.66
Σ$_{calc.}$	0.92	1.56	3.20	4.98	4.88	
Σ$_{theor.}$	1.05	1.87	3.00	5.00	5.00	

The bond valences were calculated from the bond lengths given in Table 4, and from the assigned site-populations of Table 5, with the parameters of Brown & Altermatt (1985). Some bond valences were multiplied by two (*) or by four (**) for the calculation of the valence on the Ca, P(1), and P(2) sites, and by two (***) for the calculation of the valence on the O(4) site.

and the calculated bond-lengths (CBL), respectively (Table 5). This agreement again confirms the reliability of the assigned site-populations.

Finally, the bond-valence table for bertossaite is given in Table 6, where the bond-valence sums (*b.v.s.*) were calculated as $s = \exp[(R_0 - R)/0.37]$, by using the R_0 values of Brown & Altermatt (1985). The *b.v.s.* for O(1), O(2), O(4) and O(5) are close to the theoretical value of 2.00, and the *b.v.s.* for OH(1) and OH(2) confirm their identification as OH groups. However, the low *b.v.s.* for O(3) indicates that this oxygen atom certainly plays a mixed donor–acceptor role, as it is involved in the OH(1)···O(3) hydrogen bond (see below). For the [Li(1),Li(2)], Al, P(1), and P(2) sites, a good correspondence between the theoretical and the calculated *b.v.s.* values is observed; this is not the case for the Ca site, which shows an unexpectedly low *b.v.s.* This feature is certainly related to the large volume of the CaO$_8$ site, which shares two edges with the P(1)O$_4$ tetrahedron and four edges with the AlO$_6$ octahedra. These smaller, more tightly bound polyhedra geometrically restrict the O–O shared edges (Moore & Araki 1975), and consequently do not allow the existence of short Ca–O bonds.
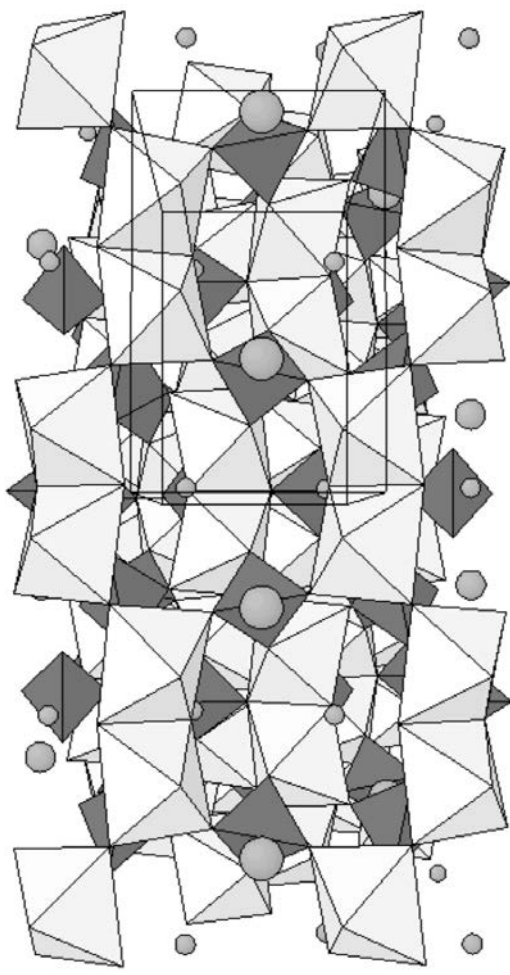
Fig. 4.   The crystal structure of bertossaite, projected along the **b** axis. For key, see Figure 3.

INFRARED SPECTRAL RESULTS

The infrared spectrum of bertossaite (Fig. 6) can be compared to the spectra of other complex orthophosphates, as for example compounds with the alluaudite (Hatert *et al*. 2003, 2005a, Hatert 2008) or wyllieite structures (Hatert *et al*. 2005b, 2006). According to the fundamental vibrational frequencies of the PO_4 tetrahedron given by Farmer (1974), the absorption bands between 941 and 1152 cm^{-1} can be assigned to ν_3, the antisymmetric stretching modes of the PO_4 anions, whereas the bands between 476 and 649 cm^{-1} can be assigned to ν_4, their bending mode.

The intense band at 762 cm^{-1} (Fig. 6) was not observed in the spectra of the anhydrous Na–Fe–Mn phosphates investigated by Hatert *et al*. (2003, 2005a, 2005b) and Hatert (2008), and corresponds to OH-bending vibrations (Farmer 1974). Similar bands, located between 720 and 840 cm^{-1}, were described in

the spectra of turquoise [$CuAl_6(PO_4)_4(OH)_8 \cdot 4H_2O$], lazulite, augelite (Moenke 1962, 1966), amblygonite [$LiAlPO_4F$], montebrasite (Fransolet & Tarte 1977), and cyrilovite [$NaFe^{3+}_3(PO_4)_2(OH)_4 \cdot 2H_2O$] (Tarte *et al*. 1984). Tarte (1958) investigated the infrared spectra of several synthetic copper salts, and established a correlation between the wavenumbers of their OH bending and stretching vibrations. Starting from the OH-bending vibration of bertossaite at 762 cm^{-1}, this correlation allows one to calculate an OH-stretching vibration of *ca.* 3550 cm^{-1}, a value in good agreement with the observed band located at 3589 cm^{-1} (Fig. 6).

The absorption bands between 2134 and 3589 cm^{-1} (Fig. 6) can be attributed to the stretching vibrations of the OH groups. Starting from the position of the two intense bands at 3397 and 3203 cm^{-1}, the correlation established by Libowitsky (1999) was used to calculate the corresponding OH···O distances, which are 2.80 and 2.71 Å, respectively. These distances are in good agree-
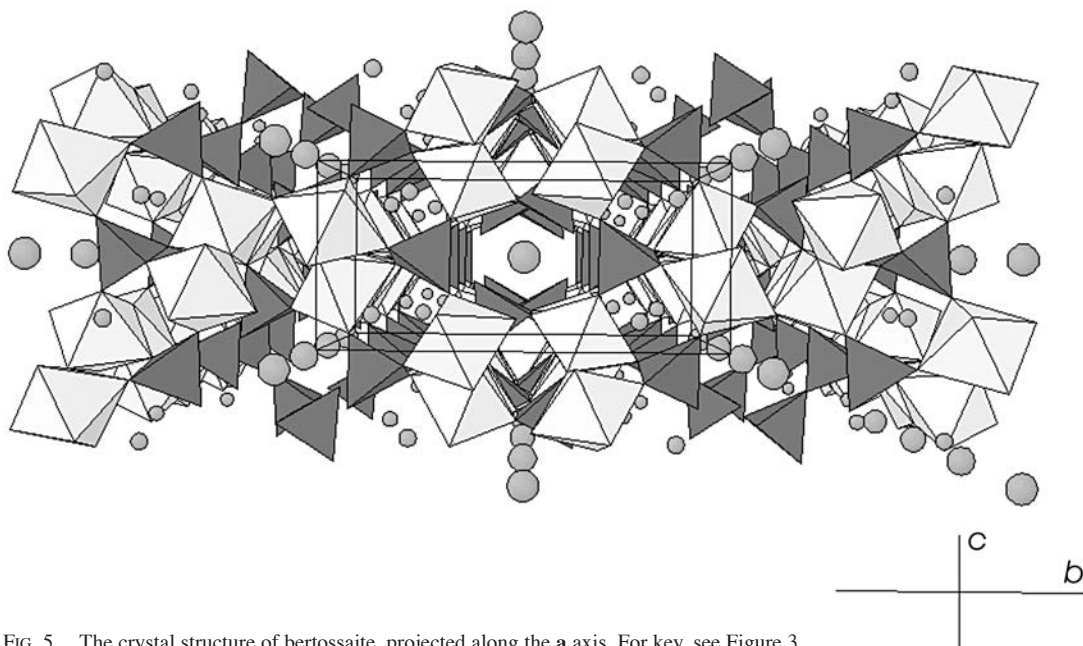
FIG. 5. The crystal structure of bertossaite, projected along the **a** axis. For key, see Figure 3.
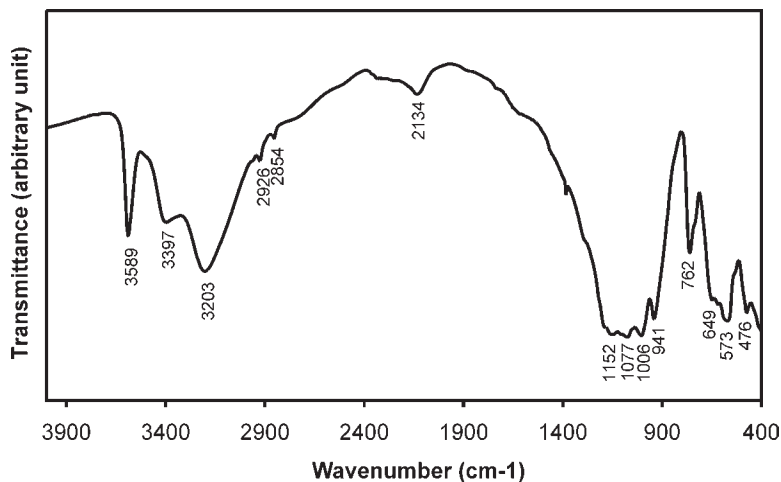

FIG. 6. The infrared spectrum of bertossaite.

ment with the OH(1)···O(3) and OH(2)···O(5) distances obtained from the structural data, which correspond to 2.669 and 2.629 Å, respectively.

DISCUSSION

The structural data given in the present paper confirm that bertossaite is isostructural with palermoite, both structures showing strong similarities with that of carminite (Olmi & Sabelli 1995, Kharisun *et al.* 1996). As shown in Table 7, the unit-cell parameters of bertossaite are significantly smaller than those of palermoite, owing to the replacement of Sr^{2+} (effective ionic radius 1.26 Å; Shannon 1976) by Ca^{2+} (*e.i.r.* 1.12 Å). Moore & Araki (1975) described the Li site of palermoite as a tetrahedron, but a recalculation of the coordination around the Li atoms in this mineral gives Li–O bond distances of 1.939, 2.002, 2.293, 2.293,

2.459, 2.839, and 2.839 Å, indicating a coordination similar to that of Li in bertossaite (Table 4). The presence of Li in large crystallographic sites is not really surprising, as Hatert *et al.* (2000, 2002) and Hatert (2004) observed this element in the 8-coordinated A(1) site (mean bond-lengths 2.52–2.63 Å) of the synthetic $(Na_{1-x}Li_x)MnFe^{3+}_2(PO_4)_3$, $(Na_{1-x}Li_x)CdIn_2(PO_4)_3$, and $(Na_{1-x}Li_x)_{1.5}Mn_{1.5}Fe^{3+}_{1.5}(PO_4)_3$ alluaudite-type solid solutions. It is noteworthy that the Li sites of bertossaite and palermoite cannot strictly be compared to the large cubic coordinated Pb(2) site of carminite, which occurs at the (0,0.25,0.25) special position (Finney 1963). The displacement of the Li site in bertossaite and palermoite induces a splitting in two equivalent positions, and a doubling of the site multiplicity, which is responsible for the presence of two Li atoms per formula unit (*apfu*) in these minerals, whereas only one Pb(2) atom occurs in carminite.

The Ca site of bertossaite can be described as a distorted cube, similar to the SrO_8 cube of palermoite (Moore & Araki 1975) and to the $Pb(1)O_8$ cube of carminite (Finney 1963). As shown in Table 7, the X(1)–O mean bond-length is positively correlated with the effective ionic radius of the cation occurring at X(1), with variations from 2.561 (bertossaite, Ca^{2+} *e.i.r.* 1.12 Å, Shannon 1976) to 2.618 Å (palermoite, Sr^{2+} *e.i.r.* 1.26 Å) and then to 2.67 Å (carminite, Pb^{2+} *e.i.r.* 1.29 Å). Calculation of bond-length distortion (BLD) coefficients (Table 7) indicates that the $Pb(1)O_8$ site of carminite is strongly distorted (BLD 7.12%); this behavior is certainly related to the presence of lone pairs of electrons in Pb^{2+} (Krivovichev & Brown 2001,

Walsh & Watson 2005). On the other hand, the SrO_8 site of palermoite shows a very low distortion-coefficient, 1.00%, thus indicating that the size of this site is fairly well adapted to the effective ionic radius of Sr^{2+}. The CaO_8 site of bertossaite is more distorted than the SrO_8 site of palermoite, with a distortion coefficient of 2.91% (Table 7). This significant distortion can be explained by the distortion theorem (Brown 2002), which states that if a cation occurs in a too large crystallographic site, then the site will distort in order to reduce the bond-valence sum for this cation. This poor fit between the size of the X(1) site and the effective ionic radius of Ca^{2+} is also responsible for the low bond-valence sum calculated for this site (Table 6).

References

Brown, I.D. (2002): *The Chemical Bond in Inorganic Chemistry*. Oxford University Press, New York, N.Y.

Brown, I.D. & Altermatt, D. (1985): Bond-valence parameters obtained from a systematic analysis of the inorganic crystal structure database. *Acta Crystallogr.* **B41**, 244-247.

Farmer, V.C. (1974): *The Infrared Spectra of Minerals*. Mineralogical Society, London. U.K. (*Monogr.* **4**).

Finney, J.J. (1963): The crystal structure of carminite. *Am. Mineral.* **48**, 1-13.

Fransolet, A.-M. & Tarte, P. (1977): Infrared spectra of analyzed samples of the amblygonite–montebrasite series: a new rapid semi-quantitative determination of fluorine. *Am. Mineral.* **62**, 559-564.

Grice, J.D. & Dunn, P.J. (1992): Attakolite: new data and crystal-structure determination. *Am. Mineral.* **77**, 1285-1291.

Hatert, F. (2004): The crystal chemistry of lithium in the alluaudite structure: a study of the $(Na_{1-x}Li_x)_{1.5}Mn_{1.5}Fe^{3+}_{1.5}(PO_4)_3$ solid solution (x = 0 to 1). *Mineral. Petrol.* **81**, 205-217.

Hatert, F. (2008): Crystal chemistry of the divalent cation in alluaudite-type phosphates: a structural and infrared spectral study of the $Na_{1.5}(Mn_{1-x}M^{2+}_x)_{1.5}Fe_{1.5}(PO_4)_3$ solid solutions (x = 0 to 1, $M^{2+} = Cd^{2+}$, Zn^{2+}). *J. Solid State Chem.* **181**, 1258-1272.

Hatert, F., Antenucci, D., Fransolet, A.-M., Liégeois-Duyckaerts, M. (2002): The crystal chemistry of

TABLE 7. SELECTED STRUCTURAL DATA FOR BERTOSSAITE AND RELATED MINERALS

		Carminite Finney (1963)	Palermoite Moore & Araki (1975)	Bertossaite This work
	a (Å)	16.595(5)	11.556(5)	11.476(1)
	b (Å)	7.580(5)	15.847(7)	15.744(1)
	c (Å)	12.295(5)	7.315(4)	7.228(1)
	β (°)	-	-	-
	V (Å³)	1546.6	1339.6	1305.9(2)
	S.G.	*Cccm*	*Imcb*	*Imcb*
X(1)	atom	Pb1	Sr	Ca
	MBL	2.67	2.618	2.561
	CN	8	8	8
	BLD	7.12	1.00	2.91
X(2)	atom	Pb2	Li	Li
	MBL	2.67	2.381	2.336
	CN	8	7	7
	BLD	7.25	9.02	8.76
M(1)	atom	Fe	Al	Al
	MBL	2.02	1.906	1.895
	CN	6	6	6
	BLD	2.72	3.60	3.37

MBL: mean bond-length, CN: coordination number, BLD: bond-length distortion, defined as $\dfrac{100}{M} \bullet \sum_{i=1}^{m} \dfrac{|d_i - d_m|}{d_m}$ (Renner & Lehmann 1986, Hatert *et al.* 2004).

lithium in the alluaudite structure: a study of the $(Na_{1-x}Li_x)$ $CdIn_2(PO_4)_3$ solid solution ($x = 0$ to 1). *J. Solid State Chem.* **163**, 194-201.

HATERT, F., HERMANN, R.P., FRANSOLET, A.-M., LONG, G.J. & GRANDJEAN, F. (2006): A structural, infrared, and Mössbauer spectral study of rosemaryite, $NaMnFe^{3+}Al(PO_4)_3$. *Eur. J. Mineral.* **18**, 775-785.

HATERT, F., HERMANN, R.P., LONG, G.J., FRANSOLET, A.-M & GRANDJEAN, F. (2003): An X-ray Rietveld, infrared, and Mössbauer spectral study of the $NaMn(Fe_{1-x}In_x)_2(PO_4)_3$ alluaudite-type solid solution. *Am. Mineral.* **88**, 211-222.

HATERT, F., KELLER, P., LISSNER, F., ANTENUCCI, D. & FRANSOLET, A.-M. (2000): First experimental evidence of alluaudite-like phosphates with high Li-content: the $(Na_{1-x}Li_x)MnFe_2(PO_4)_3$ series ($x = 0$ to 1). *Eur. J. Mineral.* **12**, 847-857.

HATERT, F., LEFEVRE, P., FRANSOLET, A.-M., SPIRLET, M.-R., REBBOUH, L., FONTAN, F. & KELLER, P. (2005b): Ferrorosemaryite, $NaFe^{2+}Fe^{3+}Al(PO_4)_3$, a new phosphate mineral from the Rubindi pegmatite, Rwanda. *Eur. J. Mineral.* **17**, 749-759.

HATERT, F., LONG, G.J., HAUTOT, D., FRANSOLET, A.-M., DELWICHE, J., HUBIN-FRANSKIN, M.J. & GRANDJEAN, F. (2004): A structural, magnetic, and Mössbauer spectral study of several Na–Mn–Fe-bearing alluaudites. *Phys. Chem. Minerals* **31**, 487-506.

HATERT, F., REBBOUH, L., HERMANN, R.P., FRANSOLET, A.-M., LONG, G.J. & GRANDJEAN, F. (2005a): Crystal chemistry of the hydrothermally synthesized $Na_2(Mn_{1-x}Fe^{2+}{}_x)_2Fe^{3+}(PO_4)_3$ alluaudite-type solid solution. *Am. Mineral.* **90**, 653-662.

KHARISUN, T.M.R., BEVAN, D.J.M. & PRING, A. (1996): The crystal structure of carminite: refinement and bond valence calculations. *Mineral. Mag.* **60**, 805-811.

KRIVOVICHEV, S.V. & BROWN, I.D. (2001): Are the compressive effects of encapsulation an artefact of the bond valence parameters? *Z. Kristallogr.* **216**, 245-247.

LEFÈVRE, P. (2003): *Contribution à l'étude minéralogique et pétrographique des associations des phosphates d'aluminium des pegmatites de Rubindi et Kabilizi (Rwanda)*. Master's thesis, University of Liège, Liège, Belgium.

LIBOWITZKY, E. (1999): Correlation of O–H stretching frequencies and O–H...O hydrogen bond lengths in minerals. *Monatsh. Chem.* **130**, 1047-1059.

MOENKE, H. (1962): *Mineralspektren I*. Akademie-Verlag, Berlin, Germany.

MOENKE, H. (1966). *Mineralspektren II*. Akademie-Verlag, Berlin, Germany.

MOORE, P.B. & ARAKI, T. (1975): Palermoite, $SrLi_2[Al_4(OH)_4(PO_4)_4]$: its atomic arrangement and relationship to carminite, $Pb_2[Fe_4(OH)_4(AsO_4)_4]$. *Am. Mineral.* **60**, 460-465.

OLMI, F. & SABELLI, C. (1995): Carminite from three localities of Sardinia (Italy). Crystal structure refinements. *Neues Jahrb. Mineral., Monatsh.*, 553-562.

RENNER, B. & LEHMANN, G. (1986): Correlation of angular and bond length distortion in TiO_4 units in crystals. *Z. Kristallogr.* **175**, 43-59.

SHANNON, R.D. (1976): Revised effective ionic radii and systematic studies of interatomic distances in halides and chalcogenides. *Acta Crystallogr.* **A32**, 751-767.

SHELDRICK, G.M. (2008): A short history of SHELX. *Acta Crystallogr.* **A64**, 112-122.

TARTE, P. (1958): Recherches sur les fréquences de déformation OH. I. Spectre infrarouge des sels basiques de cuivre. *Spectrochim. Acta* **13**, 107-119.

TARTE, P., FRANSOLET, A.-M. & PILLARD, F. (1984): Le spectre infrarouge de la cyrilovite et de la wardite: corrélations entre la structure et la composition chimique. *Bull. Minéral.* **107**, 745-754.

VON KNORRING, O. (1965): Notes on some pegmatite minerals from Rwanda. *Bull. Serv. Géol. Répúbl. Rwanda* **2**, 11-13.

VON KNORRING, O. & MROSE, M.E. (1966): Bertossaite, $(Li,Na)_2(Ca,Fe,Mn)Al_4(PO_4)_4(OH,F)_4$, a new mineral from Rwanda (Africa). *Can. Mineral.* **8**, 668 (abstr.).

WALSH, A. & WATSON, G.W. (2005): The origin of stereochemically active Pb(II) lone pair: DFT calculations on PbO and PbS. *J. Solid State Chem.* **178**, 1422-1428.